Calculation of Phase Coexistence Properties and Surface Tensions of *n*-Alkanes with Grand-Canonical Transition-Matrix Monte Carlo Simulation and Finite-Size Scaling

Jayant K. Singh and Jeffrey R. Errington*

Department of Chemical and Biological Engineering, University at Buffalo, The State University of New York, Buffalo, New York 14260-4200

Grand-canonical transition-matrix Monte Carlo is combined with configurational-bias and expanded ensemble Monte Carlo techniques to obtain saturated densities and vapor pressures of select *n*-alkanes. Surface tension values for butane, hexane, and octane are also computed via the finite-size scaling method of Binder. The exponential-6 model of Errington and Panagiotopoulos is used to describe the molecular interactions. The effect of the number of configurational-bias trial conformations on the efficiency of phase equilibra calculations is studied. We find that a broad range of trial conformation numbers give reasonable performance, with the optimal value increasing with decreasing temperature for a fixed chain length. Phase coexistence properties are in good agreement with literature values and are obtained with very reasonable computing resources. Similar to other recently developed *n*-alkane force fields, the exponential-6 model overestimates the surface tension relative to experimental values. Statistical uncertainties for coexistence properties obtained with the current approach are relatively small compared to existing methods.

I. Introduction

Hydrocarbons and their derivatives are abundant in nature. These molecules are used in numerous chemical processes and play an important role in many biological applications. Several oils, fats, solvents, waxes, and paraffins consist of either hydrocarbon molecules or species containing large hydrocarbon units. In the chemical industry hydrocarbons are used as feedstock in the production of petroleum, natural gas, and other fuels. Hydrocarbons are also found in many personal care products, such as moisturizers, makeup, and lip balm. Due to the widespread use of hydrocarbons it is desirable to have a rapid and precise means to evaluate their saturation and interfacial properties.

The ability to calculate directly the phase diagram of molecular models is perhaps one of the most important outcomes of advances in molecular simulation techniques over the past couple of decades. Improvements in computing power and algorithms have made molecular simulation a very attractive tool for calculating phase coexistence and other thermophysical properties. Introduction of the Gibbs ensemble Monte Carlo method (GEMC) by Panagiotopolous[1] greatly enhanced our ability to predict the phase behavior of real and model systems. However, it was not until GEMC was combined with a biased sampling scheme, configurational-bias,[2–6] that the technique could be used to evaluate the saturation properties of *n*-alkane chains of moderate length. One of the trial moves in GEMC involves the exchange of particles between the vapor and liquid phase. This particular trial move has a very low acceptance rate for chain molecules since random insertion of a chain molecule from a vapor to liquid phase almost always results in overlap. As a result, a prohibitively large number of trial insertions are required to correctly sample the coexisting phases of chain systems. The configurational-bias Monte Carlo algorithm (CBMC)

was devised to explore configuration space more efficiently. In this method, instead of random insertion, a molecule is grown atom by atom, with multiple conformations examined for a given atom, such that the probability of finding regions of favorable energy is enhanced, and the likelihood of molecules overlapping is reduced. Gibbs ensemble Monte Carlo in combination with CBMC has been applied successfully to determine the coexistence properties of many systems, including alkanes[6,7] and Lennard-Jones chains.[8]

Another algorithm, expanded ensemble Monte Carlo (EE-MC),[9] was also developed to overcome sampling difficulties for long chains (e.g., polymers). In this approach, molecules are gradually inserted and deleted through a series of intermediate states. At any given instance the system consists of any number of completely grown molecules and at most one tagged molecule that exists in one of the intermediate states. Trial moves are performed to increase or decrease the length of the tagged molecule until it is either completely added to or deleted from the system. Escobedo and de Pablo demonstrated how to implement this approach within the grand canonical ensemble to determine thermophysical properties of chain systems.[9]

Considerable work has been completed to determine the ability of various molecular models to accurately predict the phase coexistence properties (saturated densities, vapor pressures) of *n*-alkane systems.[10–15] Comparatively less attention has been given to asses the ability of these models to correctly predict surface tensions.[16] Alejendre et al.[16] have computed the vapor–liquid surface tension of *n*-hexane using both the de Pablo et al.[11] and SKS[7] models. More recently, Nicolos and Smit[17] reported the surface tension of select *n*-alkanes using the OPLS[10] and SKS[12] force fields. Both of these research groups performed molecular dynamics simulations with a slab geometry[18] to obtain surface tension estimates. In addition, both groups modified the true force field by truncating and shifting the potential at a given cutoff distance. Using this approach, the authors found that model predictions underestimated the

---

* To whom correspondence should be addressed. E-mail: jerring@buffalo.edu.

surface tension relative to experimental data. Goujon et al.[19] performed a series of slab-based calculations using the TraPPE model[13] in which the long-range interactions were explicitly accounted for. Their results indicated that the true TraPPE force field slightly overestimates the surface tension of *n*-pentane.

In previous work, one of us introduced a new method, grand-canonical transition-matrix Monte Carlo (GC-TMMC),[20] for locating and characterizing fluid phase transitions. With this approach, simulations are conducted in a standard grand canonical ensemble where the volume, chemical potential, and temperature are held constant and the particle number (density) and energy fluctuate. During a simulation attempted transitions between states of different density are monitored as opposed to tracking the number of times the chain visits a given density as is done in conventional simulations.[21,22] At regular intervals during a simulation, this information is used to obtain an estimate of the density probability distribution, which is subsequently used to bias the sampling[23] to low probability densities. Over time all densities of interest are sampled adequately. The end result is an efficient self-adaptive method for determining the density probability distribution over a specified range of densities (typically a range that corresponds to the densities of two potentially coexisting phases). Once a probability distribution has been collected at a given value of the chemical potential, histogram reweighting[24] is used to shift the probability distribution to other values of the chemical potential. Phase coexistence is located when a chemical potential is identified that produces equal areas under the peaks in a bimodal density probability distribution.

In addition to the calculation of saturation pressures, densities, and energies, grand-canonical Monte Carlo simulation can also be combined with finite-size scaling methods to evaluate surface tension values. This method does not require completion of the often difficult task of establishing, equilibrating, and then maintaining an interface, as is required in slab-based methods. In the grand-canonical approach surface tension values are calculated by using the finite-size scaling technique of Binder.[25] In this formalism, apparent system-size-dependent interfacial tensions are calculated for a range of system sizes, which are subsequently used to extrapolate the infinite-system-size surface tension through finite-size scaling. This approach has now been applied to obtain the surface tension of various fluids.[26−29]

In this work we extend the application of GC-TMMC to systems containing chain molecules. This task is accomplished by combining GC-TMMC with CBMC and EEMC methods to calculate phase coexistence properties and surface tension values for normal alkanes. The number of trial orientations attempted for each interaction site is a variable common to both the CBMC and EEMC methods. Here, we investigate the effect of this quantity on the rate of convergence of the density probability distribution. The formalism of Binder has been used primarily to obtain surface tensions for monatomic systems. The application of this approach to molecular systems is studied here. In particular, we examine the range of system sizes required to accurately determine surface tension values. The rest of the paper is organized as follows. Section II outlines the methods used in this study. Section III describes the potential model and outlines the simulation details. In section IV, we present the results of our investigation, and we conclude in section V.

II. Methodology

We begin by reviewing the general GC-TMMC approach for calculating phase coexistence properties and surface tension values, and next describe how to incorporate configurational-bias and expanded ensemble techniques into the scheme. Simulations are conducted in a grand canonical ensemble in which the chemical potential μ, volume V, and temperature T are kept fixed and particle number N and energy U fluctuate. The probability π of observing a microstate s with energy U and particle number N is

$$\pi_s = \frac{1}{\Xi} \frac{q(T)^{N_s} V^{N_s}}{N_s!} \exp[-\beta(U_s - \mu N_s)] \quad (1)$$

where β is the inverse temperature ($\beta = 1/k_B T$, k_B is Boltzmann factor), Ξ is the grand partition function, and $q(T)$ is the kinetic contribution to the molecular partition function. The probability $\Pi(N)$ of observing a macrostate with a given number of molecules (density) is given by

$$\Pi(N) = \sum_{N_s = N} \pi_s \quad (2)$$

To obtain the probability distribution $\Pi(N)$ we employ a transition matrix Monte Carlo scheme,[21] with an N-dependent sampling bias. The method monitors the acceptance probability of attempted MC moves and subsequently uses this information to calculate the macrostate transition probability matrix. For every attempted move from a microstate s to a microstate t, regardless of whether the move is accepted, we update a collection matrix C with the acceptance probability $a(s{\rightarrow}t) = \min[1, \pi_t/\pi_s]$ as follows

$$C(N{\rightarrow}M) = C(N{\rightarrow}M) + a(s{\rightarrow}t)$$

and

$$C(N{\rightarrow}N) = C(N{\rightarrow}N) + 1 - a(s{\rightarrow}t) \quad (3)$$

where N and M represent the macrostate labels for microstates s and t, respectively. At any time during the simulation the macrostate transition probability matrix can be obtained by appropriately normalizing the collection matrix

$$P(N{\rightarrow}M) = \frac{C(N{\rightarrow}M)}{\sum_O C(N{\rightarrow}O)} \quad (4)$$

To obtain the macrostate probabilities, we utilize the detailed balance expression

$$\Pi(N)P(N{\rightarrow}M) = \Pi(M)P(M{\rightarrow}N)$$

For a grand-canonical simulation where transitions in N are such that $N \rightarrow N$, $N \rightarrow N + 1$, and $N \rightarrow N - 1$, the transition-probability matrix P is tri-diagonal. In such conditions, a sequential approach provides a suitable means for obtaining the macrostate probabilities

$$\ln \Pi(N+1) = \ln \Pi(N) - \ln\left[\frac{P(N+1{\rightarrow}N)}{P(N{\rightarrow}N+1)}\right] \quad (5)$$

At coexistence the macrostate probability distribution shows two peaks as shown in Figure 1. The peaks correspond to stable (or metastable) homogeneous phases and the intermediate-density region corresponds to homogeneous or heterogeneous configurations. As is suggested in Figure 1, obtaining a particle number probability distribution over a range of densities that includes liquid and vapor states requires sampling density regions of low probability. To ensure adequate sampling of all
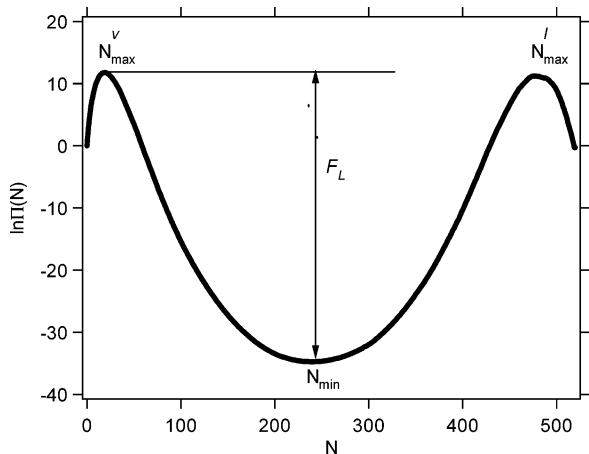
Evaluation of the Saturation Properties of *n*-Alkanes

J. Phys. Chem. B, Vol. 110, No. 3, 2006 **1371**

Figure 1. Schematic of the particle number probability distribution at vapor−liquid phase coexistence conditions.

states we employ a multicanonical sampling[23] scheme that encourages the system to sample all densities with uniform frequency. This procedure is implemented by assigning each macrostate a weight $\eta(N)$ that is inversely proportional to the current estimate of its probability, $\eta(N) = -\ln \Pi(N)$. Acceptance criteria are modified to account for the bias as follows

$$a_\eta(s \rightarrow t) = \min\left[1, \frac{\exp[\eta(M)]\pi_t}{\exp[\eta(N)]\pi_s}\right] \qquad (6)$$

where $\eta(N)$ and $\eta(M)$ are weights corresponding to microstates s and t, respectively. Note that the introduction of a weighting function does not alter the mechanism through which the collection matrix is updated. The unbiased acceptance probability is still used to update the collection matrix. This aspect of the method provides an efficient and self-adaptive means to determine the probability distribution by enabling one to periodically update the weighting function without having to discard previously obtained data in the collection matrix.

Simulations are completed at a specified value of the chemical potential, which does not need to be particularly close to the saturation value. To determine the phase-coexistence value of the chemical potential, the histogram reweighting method of Ferrenberg and Swendsen[24] is used. This method enables one to shift the probability distribution obtained from a simulation at chemical potential μ_o to a probability distribution corresponding to a chemical potential μ using the relation

$$\ln \Pi(N; \mu) = \ln \Pi(N; \mu_o) + \beta(\mu - \mu_o)N \qquad (7)$$

To determine the coexistence chemical potential, we apply the above relation to find the chemical potential that produces a probability distribution $\Pi_c(N)$, where the areas under the vapor and liquid regions are equal. Saturated densities are related to the first moment of the vapor and liquid peaks of the coexistence probability distribution. To calculate the saturation pressure we use the expression

$$\beta pV = \ln\left(\sum_N \Pi_c(N)/\Pi_c(0)\right) - \ln(2) \qquad (8)$$

The interfacial free energy F_L for a finite-size system with a cell length of L is determined from the maximum likelihood in the liquid $\Pi^l_{\max}$ and vapor regions $\Pi^v_{\max}$ and minimum likelihood in the interface region $\Pi_{\min}$ (see Figure 1),

$$\beta F_L = \frac{1}{2}(\ln \Pi^l_{\max} + \ln \Pi^v_{\max}) - \ln \Pi_{\min} \qquad (9)$$

From the formalism of Binder,[25] the interfacial free energy of a two-dimensional surface varies with system size according to

$$\beta \gamma_L = \frac{\beta F_L}{2L^2} = C_1 \frac{1}{L^2} + C_2 \frac{\ln L}{L^2} + \beta \gamma_\infty \qquad (10)$$

where γ_L is an apparent system-size-dependent surface tension, γ_∞ is the true infinite-system ($L \rightarrow \infty$) interfacial tension, and C_1 and C_2 are constants. The expression suggests that the group $\beta F_L/2L^2$ becomes linear with the scaling variable $\ln(L)/L^2$ as the system size approaches infinity. The method enables one to evaluate the infinite-system interfacial tension by extrapolating a series of finite-system interfacial free energies.

We now examine how to include configurational-bias and expanded ensemble techniques within the GC-TMMC framework. The CBMC routine can be incorporated in a relatively straightforward manner. We recognize that the TMMC algorithm does not distinguish between elementary and advanced moves. Rather, it requires only the acceptance probability between two microstates involved in the trial move. For the case of CB-GCMC, the acceptance probabilities for particle insertions and deletions are given by[30]

$$a(N \rightarrow N+1) = \min\left(1, \frac{q(T)V \exp(\beta\mu)}{(N+1)} R_w(\text{new})\right)$$

$$a(N \rightarrow N-1) = \min\left(1, \frac{N}{q(T)V \exp(\beta\mu)} \frac{1}{R_w(\text{old})}\right) \quad (11)$$

where R_w is the Rosenbluth weight, which is calculated as described by Frenkel and Smit.[30]

In expanded grand-canonical Monte Carlo the creation and deletion of molecules is completed through a series of intermediate stages. At any point during the simulation the system consists of any number of completely grown molecules and at most one partially grown molecule, referred to as the tagged molecule. The tagged molecule keeps its label until it is grown to a full molecule or completely eliminated. Within this approach each intermediate state containing a partially grown molecule is considered a unique macrostate. For a simulation designed to obtain the particle number probability distribution between zero and $N_{\max}$ particles, the number of macrostates is now $nN_{\max} + 1$, where n is the number of steps required to grow a complete molecule. As before, transitions are attempted that move the system to one of two neighboring macrostates. For a system containing a tagged molecule in the yth growth stage, creation and deletion moves involve attempted transitions to states $y + 1$ and $y - 1$, respectively. The acceptance probability for a move from state y to state $y + \Delta$ is given by

$$a(y \rightarrow y+\Delta) = \min\left(1, (R_w)^\Delta \exp\left(\frac{\Delta}{n}\left[\beta\mu - \ln\frac{N_y}{q(T)V}\right]\right)\right) \quad (12)$$

where Δ is $+1$ for the growth process and -1 for the destruction process, N_y is the total number of molecules in the system including the tagged chain, and R_w is the Rosenbluth weight.[9]

III. Model and Simulation Details

A united-atom approach is used to model the *n*-alkane molecules. We focus on the exponential-6 model of Errington and Panagiotopoulos. Details related to other united-atom

models discussed below can be found elsewhere. Nonbonded site−site interactions are described with the modified Buckingham exponential-6 intermolecular potential,[15] for which pair interaction energies u vary with separation distance r as

$$u(r) = \begin{cases} \dfrac{\epsilon}{1 - 6/\alpha}\left[\dfrac{6}{\alpha}\exp\left(\alpha\left[1 - \dfrac{r}{r_m}\right]\right) - \left(\dfrac{r_m}{r}\right)^6\right] & \text{for } r > r_{\max} \\ \infty & \text{for } r < r_{\max} \end{cases}$$

(13)

where ϵ, r_m, and α are adjustable parameters. The variable r_m is the radial distance at which $u(r)$ reaches a minimum and the cutoff distance $r_{\max}$ is the smallest radial distance for which $du/dr = 0$. The radial distance for which $u(r) = 0$ is denoted by σ. The parameters ϵ, σ, and α are 129.63 K, 3.679 Å, and 16, respectively, for the methyl group and 73.5 K, 4.00 Å, and 22, respectively, for the methylene group. Cross parameters are determined by using the following combining rules,

$$\sigma_{ij} = \frac{1}{2}(\sigma_i + \sigma_j)$$

$$\epsilon_{ij} = (\epsilon_i\epsilon_j)^{1/2}$$

$$\alpha_{ij} = (\alpha_i\alpha_j)^{1/2}$$

(14)

The bond lengths CH_3-CH_3, CH_3-CH_2, and CH_2-CH_2 are 1.839 Å, 1.687 Å, and 1.535 Å, respectively. Bond bending angles are generated according to the bending potential[31]

$$u_{\text{bend}}(\theta) = \frac{K_\theta}{2}(\theta - \theta_{\text{eq}})^2$$

(15)

where $K_\theta = 62500$ K/rad^2 and $\theta_{\text{eq}} = 114°$. Torsion angles are generated according to the potential[12]

$$u_{\text{tor}}(\phi) = V_0 + \frac{V_1}{2}(1 + \cos\phi) + \frac{V_2}{2}(1 - \cos 2\phi) + \frac{V_3}{2}(1 + \cos 3\phi)$$

(16)

where $V_0 = 0$, $V_1 = 355.03$ K, $V_2 = -68.19$ K, and $V_3 = 791.32$ K.

Simulations for calculating saturated densities and vapor pressures are conducted with use of a single 1.0 GHz Pentium III processor. The MC move distribution is as follows: 15% particle displacement, 50% particle insertion/deletion, 15% particle rotation, and 20% partial regrowth. Typical maximum molecule numbers for these simulations span from around 150 (for dodecane) to 500 (for methane). Surface tension extrapolations require relatively large system sizes. For these simulations the largest systems considered contained a maximum of around 2200 molecules. To perform these calculations in an efficient manner we take advantage of the fact that the TMMC algorithm enables one to fill the overall collection matrix through a series of independent simulations, each restricted to a limited range of macrostate space. There are a variety of ways that one can implement this parallelization in practice. In this work, we use a scheme in which a series of semi-independent simultaneous simulations sample overlapping windows in macrostate space with periodic swapping of configurations between processors. Further details can be found in ref 32, where this windowing approach was used to determine the phase behavior of a fluid interacting with a surface. While we feel that this approach is
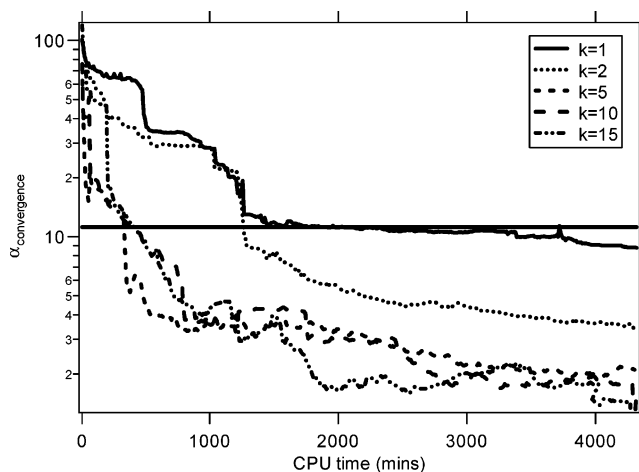

Figure 2. Probability distribution convergence plot for octane at $T = 500$ K. The horizontal line indicates a target value for convergence.

reasonable, we recognize that the mechanism used to distribute the workload between processors could be optimized further. The issue of load balance among multiple processors is of general interest for TMMC applications and would likely benefit from further study.

IV. Results and Discussion

Appropriate selection of the number of configurational-bias trial orientations k can significantly improve the efficiency of grand-canonical simulations. Here we investigate the effect of k on the rate of convergence of the density probability distribution. Phase coexistence calculations for n-octane at 400 and 500 K are taken as test cases. Two metrics are used to track convergence. For the first measure, convergence is assessed by examining the deviation between instantaneous and target probability values for each element of the distribution. Multiple runs are performed to obtain good statistics with the following expression used to acquire an average result

$$\alpha_{\text{convergence}}(t) = \sqrt{\frac{1}{M_{\text{run}}}\sum_{j=1}^{M_{\text{run}}}\sum_{i=N_{\text{min}}}^{N_{\text{max}}}[\ln\Pi(i,t) - \ln\Pi_{\text{tar}}(i)]^2}$$

(17)

where t is the elapsed CPU time, Π and Π_{tar} are the instantaneous and target density probability distributions normalized to sum to unity, M_{run} is the number of runs, and N_{min} and N_{max} are the minimum (zero in the present study) and maximum number of particles sampled. Target probability distributions are generated from 64 independent simulations with a k value of 8.

To assess the influence of the number of trial orientations on the rate of convergence, we performed a series of simulations in which the value of k was varied from 1 to 20. Simulations were conducted with a volume of $V = 40\,000$ Å^3, using 1.0 GHz Pentium III processors. Results for $\alpha_{\text{convergence}}$ as a function of CPU time for $T = 500$ K are displayed in Figure 2. The run length was truncated at around 4000 min. We observe that for $k \geq 5$ convergence is achieved satisfactorily within 400 min of CPU time, whereas for $k = 1$ and 2, 1300 and 2400 min of simulation time are required, respectively. It is clear that the use of configurational-bias significantly influences the rate of convergence. The data indicate that the rate of convergence remains relatively constant for k values above 5, suggesting that one has fairly wide latitude in selecting an optimal k value at this temperature.

Evaluation of the Saturation Properties of *n*-Alkanes

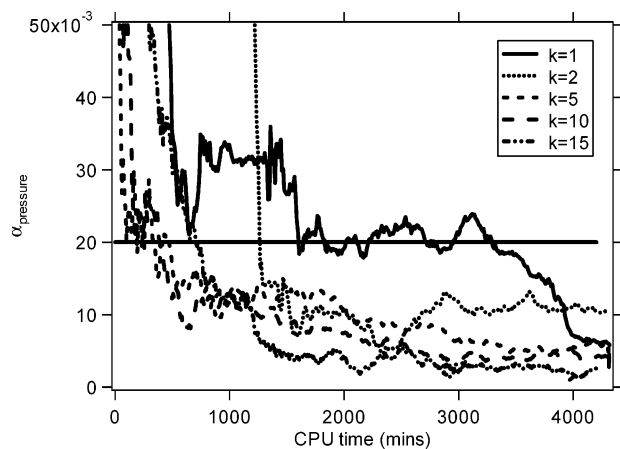*J. Phys. Chem. B, Vol. 110, No. 3, 2006* **1373**

Figure 3. Absolute fractional difference between the instantaneous and target pressure against the CPU time for octane at $T = 500$ K. The horizontal line indicates a target value for convergence.

The second metric used to track the rate of convergence of the density probability distribution focuses on the evolution of the pressure with simulation time. The pressure is related to the zeroth moment of the probability distribution (see eq 8), and therefore represents an aggregate property of the distribution. The metric $\alpha_{pressure}$ is defined in terms of the difference between an instantaneous P and target P_{tar} value of the pressure

$$\alpha_{pressure}(t) = \frac{1}{M_{run}} \sum_{j=1}^{M_{run}} \frac{|P(t) - P_{tar}|}{P_{tar}}$$

The evolution of $\alpha_{pressure}$ with CPU time for the same k values examined above is displayed in Figure 3. The behavior is similar to what we observed for the first metric, i.e., values of $k \geq 5$ increase significantly simulation efficiency. Although differences between the $k = 5$, 10, and 15 data sets are small, k values of 5 and 10 seem to slightly outperform the $k = 15$ case. However, as indicated, these differences are relatively small and we again find that a broad range for k values produces equivalent results.

It is well-known that temperature has a tremendous influence on the rate with which a system evolves through configuration space. To probe the effect of temperature on the optimal number of configurational-bias trial orientations we monitored the same metrics described above for phase equilibria calculations conducted at a temperature of $T = 400$ K. Results for $\alpha_{convergence}$ as a function of CPU time are displayed in Figure 4. It is evident that a k value of 5 is no longer optimal. For k values even lower than 5, convergence requires considerably longer run times. Relatively similar performance is found when using 10, 15, or 20 trial orientations, with $k = 10$ producing the best result. Analogous to the high-temperature case, a broad range of k values can be used to obtain phase coexistence data in an efficient manner. Similar conclusions are obtained from an analysis of the dependence of $\alpha_{pressure}$ with CPU time. The two test cases indicate that k values of 5 or larger are preferable at a reduced temperature of 0.88 and that 10 or more trial orientations provide optimal convergence rates at a reduced temperature of 0.70. Both test cases indicate that the rate of convergence initially increases rapidly with increasing trial orientations. This early period is followed by a weak maximum in the convergence rate with increasing k values. Therefore, when selecting the number of trial orientations for GC-TMMC simulations one should error on the side of larger rather than optimal k values.

After obtaining a sense of how the number of trial orientations influences convergence rates, we used the GC-TMMC method
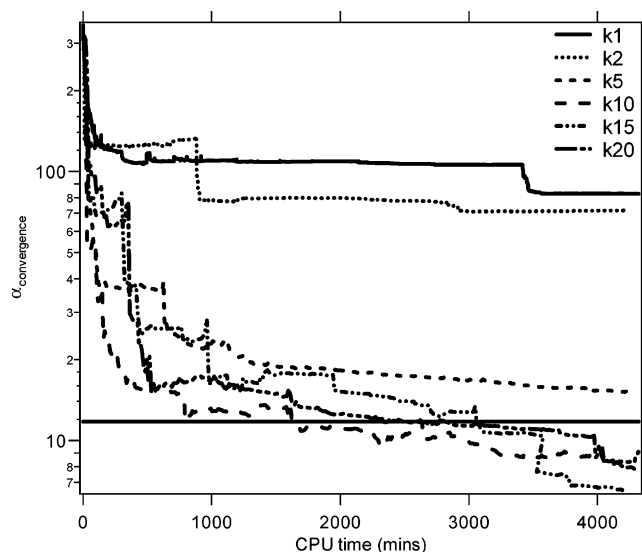

Figure 4. Probability distribution convergence plot for octane at $T = 400$ K. Details are equivalent to those for Figure 2.
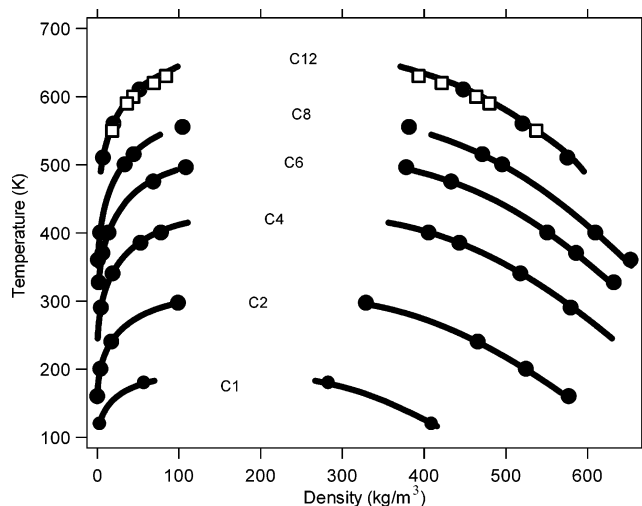

Figure 5. Vapor–liquid coexistence envelope of select *n*-alkanes. The curves from bottom to top are for methane, ethane, butane, hexane, octane, and dodecane. Solid lines represent literature values,[15] filled circles represents data obtained with CB-GC-TMMC, and open squares represent data obtained with EE-GC-TMMC. Statistical uncertainties are smaller than the symbol size.

to determine phase coexistence properties for a wide range of chain lengths. Saturated densities and vapor pressures for select *n*-alkanes are displayed in Figures 5 and 6, respectively. A set of coexistence calculations was completed for each molecule with use of CB-GC-TMMC. For dodecane an additional series of simulations was conducted with the EE-GC-TMMC method. Results from the present study are in very good agreement with the values of Errington and Panagiotopoulos.[15] All phase coexistence calculations were completed by using a single 1.0 GHz Pentium III processor and required less than 3 days of simulation time. As one would expect, simulations involving relatively short chains and/or relatively high temperatures required considerably less time to complete. Four runs were conducted at each state point to evaluate statistical uncertainties. We found typical uncertainties of less than 1% for the saturated densities and vapor pressures. These values are considerably smaller than vapor pressure uncertainties commonly obtained from Gibbs ensemble simulations.[12]

One of the advantageous aspects of the GC-TMMC method is that it can be used in conjunction with finite-size scaling (FSS)
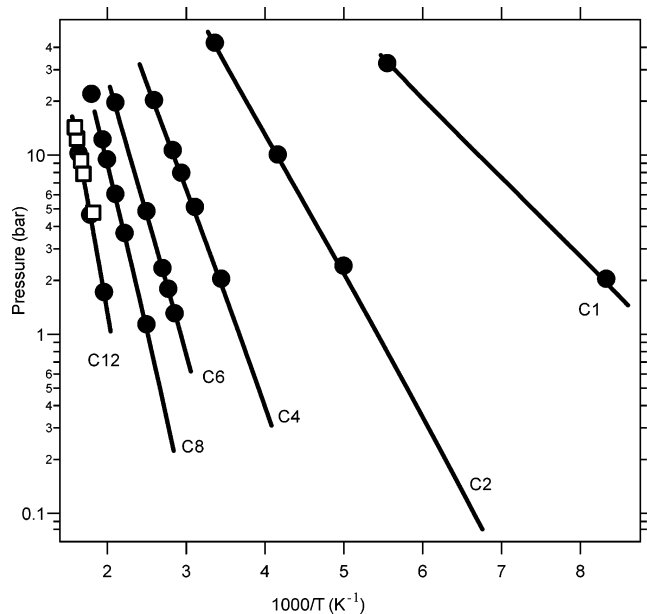
Figure 6. Vapor pressure of select *n*-alkanes. The curves from right to left are for methane, ethane, butane, hexane, octane, and dodecane. Symbols are the same as in Figure 5.

Figure 7. Apparent surface tension values of modified SKS hexane as a function of the scaling variable. The soild symbols represent system-size-dependent TMMC-FSS results and the open symbols correspond to slab-based values from Nicolas and Smit.[17] The lines provide an extrapolation of TMMC-FSS data to the infinite-system limit, with the solid line indicating those points that were used in the extrapolation, and the dotted line representing an extension of the extrapolation to smaller system sizes.

ideas proposed by Binder to produce a powerful means for determining surface tension values. This approach is particularly appealing at near-critical temperatures where slab-based methods face difficulties in maintaining a stable interface. Recently, Singh et al.[27] have demonstrated the effectiveness of this technique relative to alternative slab-based methods in which the pressure tensor is evaluated either through the virial or volume perturbation. The approach also benefits from the ease with which calculations can be performed with parallel processing. For example, this aspect of the method has proven to be useful when working with anisotropic potentials.[28,29] The combined TMMC-FSS method has been used to determine surface tension values for Lennard-Jones,[20] square-well,[27] and model associating fluids.[28] In this work, we examine the suitability of this method for obtaining surface tension values of chain molecules.

At the outset of the surface tension study, we performed a series of calculations to compare *n*-alkane surface tension values obtained from the TMMC-FSS method to those determined from a traditional slab-based approach. We initially focused on a system investigated by Nicolas and Smit.[17] These authors calculated surface tension values for hexane using a modified SKS model.[7] The force field was modified by truncating and shifting the site−site interaction potential with a cutoff distance of 13.8 Å. By modifying the potential in this manner, one does not have to address the various issues related to the long-range nature of the potential. Below, we examine the case in which the full potential is used. Nicolas and Smit obtained surface tension values by integrating the difference between normal and tangential components of the pressure tensor over the axis perpendicular to the interface. The pressure tensor was evaluated by using the Irving and Kirkwood definition[18] during molecular dynamics simulations. In Figure 7 we present our apparent size-dependent surface tension estimates as a function of the scaling variable at temperatures of 350, 400, and 450 K. These values are extrapolated to the infinite-system limit and compared with the values of Nicolas and Smit. At temperatures of 350 and 450 K, values from the two methods are in very good agreement. At the intermediate temperature of 400 K, the TMMC-FSS result is just outside the uncertainty bounds of the slab-based calculation. However, we feel that our result at 400 K is reasonable,
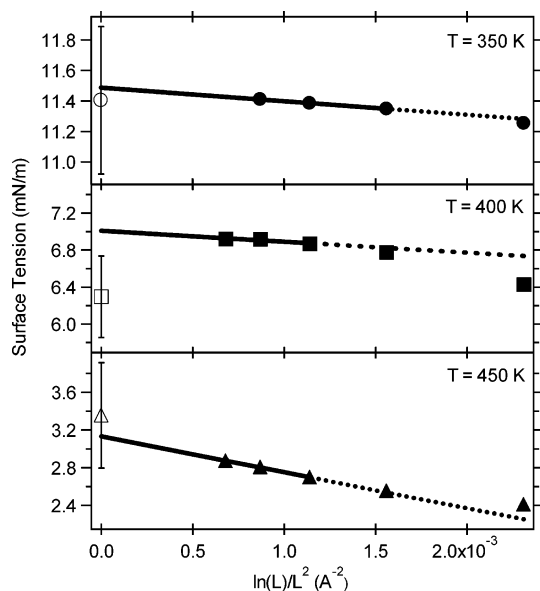
in that it is in good agreement with the value one obtains from a linear interpolation of the slab-based results at 350 and 450 K. One of the noticeable differences between the two methods is the magnitude of the uncertainty in the calculated interfacial tension. Typical uncertainties for values obtained with the slab-based approach are around 10%, whereas those for values generated from the TMMC-FSS method are under 2%.

To obtain a better understanding of the role long-range interactions play in evaluation of the surface tension, we next examined the interfacial properties of an alkane system previously studied by Goujon et al.[19] These authors performed a number of slab-based calculations with the TraPPE model for *n*-pentane in which the potential cutoff distance and system size were varied. Similar to Nicolas and Smit's work, the pressure tensor was evaluated by using the Irving and Kirkwood definition; however, Goujon et al. implemented Monte Carlo instead of molecular dynamics simulations to sample configuration space. In the present study, we examine how true surface tension values obtained from the TMMC-FSS method evolve with the potential cutoff distance. Apparent surface tension values are calculated with system sizes of $L = 50$, 60, and 70 Å for several cutoff distances, and these data are subsequently used to extract true surface tensions. Data obtained from this procedure are displayed in Figure 8, along with the values obtained by Goujon et al. It is clear that the cutoff distance has a significant impact on the interfacial tension. The results indicate that the magnitude of the surface tension decreases with increasing cutoff distance, with the estimates eventually converging to a common value. For cutoff distances of 20 Å (approximately five alkane segment diameters) and larger, one obtains a surface tension value that is within 3.5% of the value generated with the maximum possible cutoff distance (half the box length). True surface tension values obtained with a relatively large cutoff distance are also in good agreement with the slab-based results of Goujon et al. The data suggest that the TMMC-FSS method can be used to produce surface tension
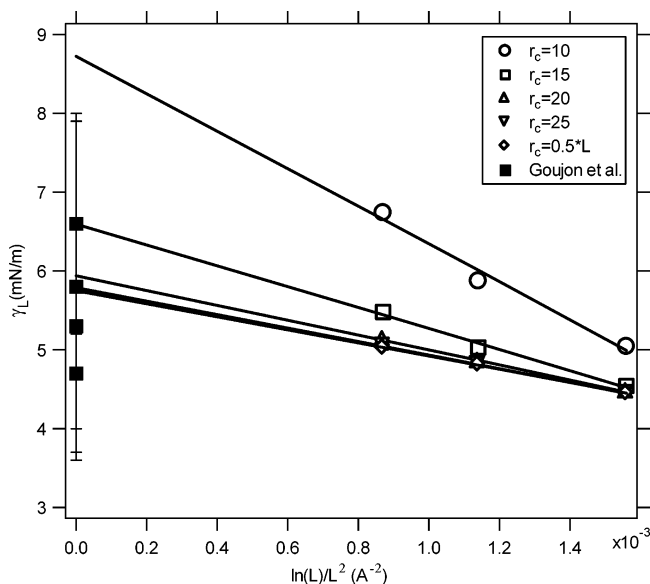
Evaluation of the Saturation Properties of *n*-Alkanes

J. Phys. Chem. B, Vol. 110, No. 3, 2006 **1375**

Figure 8. Apparent surface tension values for TraPPE hexane at 400 K as a function of the scaling variable. Open symbols represent system-size-dependent values obtained by applying the TMMC-FSS approach with various cutoff distances. The filled squares correspond to values obtained by Goujon et al.[19] from slab-based calculations, with each point representing a unique system size−cutoff distance combination.

values, which are consistent with slab-based approaches, for molecular models that contain long-range interactions.

One of the objectives of the current study was to determine the range of system sizes required for accurate determination of surface tensions for model chain systems. In previous work with atomistic systems, we found that apparent surface tension values scaled linearly with the scaling variable for system sizes of approximately $L = 9\sigma$ and larger.[20,33] In these studies, extrapolations were performed with data collected from three to five systems with cell dimensions between roughly $L = 9\sigma$ and 14σ. This range of system sizes corresponds to a maximum number of particles that spans from approximately 600 to 2000. On the basis of the data presented in Figures 7 and 8, it appears that one needs to consider a similar maximum particle number range for the relatively short chain systems examined here. For example, the finite-size scaling for SKS *n*-hexane at 400 K was completed by using three system sizes with N_{max} values of 864, 1358, and 2012.

Depending on the level of accuracy one is interested in, a full finite-size scaling analysis may not be required at all temperatures. Similar to what was found for the atomistic case,[20,33] we find that the magnitude of the slope of the scaling line increases with increasing temperature. Stated differently, the fractional difference between an apparent surface tension value calculated with a given system size and the true extrapolated value increases with the saturation temperature. As an illustrative example, consider the scaling for SKS *n*-hexane, for which the fractional difference between the apparent $L = 60$ ($N_{max} \sim 850$) and the true surface tension value increases from 1% to 14% as the temperature increases from 350 to 450 K. This result suggests that one can obtain surface tensions at relatively low reduced temperatures that are accurate to within a few percent without performing a full finite-size scaling analysis. For example, by simply using the apparent $L = 60$ value for the surface tension of SKS *n*-hexane at 350 K, one would underestimate the surface tension by just 1%.

Finally, we examine the ability of the Errington and Pana-giotopoulos exponential-6 model to accurately describe the
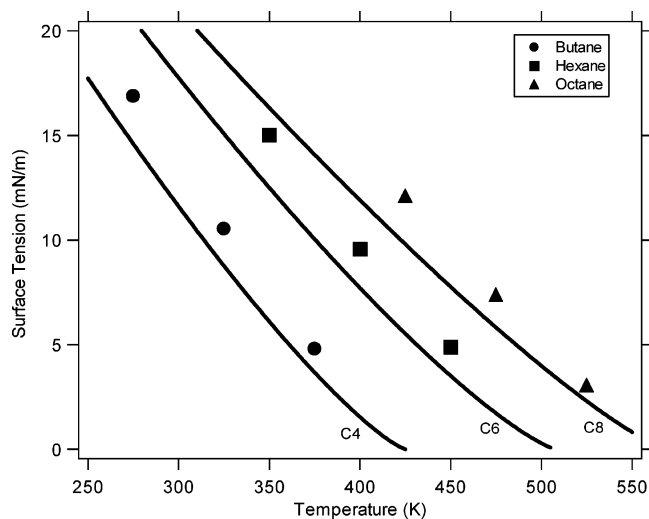

Figure 9. The surface tension of butane, hexane, and octane plotted as a function of temperature. Lines represent experimental values[34] and symbols represent predictions from the exponential-6 model.

interfacial tension of select *n*-alkanes. Model predictions and experimental data[34] for the surface tension of *n*-butane, *n*-hexane, and *n*-octane are displayed in Figure 9. Results for butane, hexane, and octane were obtained by scaling three apparent surface tension values evaluated with system sizes of (50, 60, 70), (55, 65, 75), and (65, 75, 85) Å, respectively. All apparent surface tensions were calculated by using a potential cutoff distance of 25 Å. It is clear that the exponential-6 model overestimates the surface tension. The average deviation between model and experimental points is 26%. For comparison, data for the TraPPE *n*-pentane model at 400 K presented in Figure 8 correspond to a surface tension of 5.79 mN/m, which is 13% larger than the experimental value. This deviation is consistent with those reported by Goujon et al.[19] for the TraPPE *n*-pentane model at other temperatures.

V. Conclusion

We have studied the applicability of grand-canonical transi-tion-matrix Monte Carlo for determining phase coexistence properties of normal alkanes. Configurational-bias Monte Carlo and expanded ensemble techniques were combined with the original GC-TMMC formalism to produce an efficient and self-adaptive method for evaluating thermophysical properties. We found that when using this method saturation properties were generated to within 1% uncertainty, and that the values were in good agreement with literature values. In addition, CPU time requirements were reasonable in all cases. Studies aimed at understanding the optimal number of configurational-bias trial orientations (k) indicated that the rate of convergence of the density probability distribution initially increases rapidly with k, after which one observes a weak maximum in the convergence rate upon further increasing k. As one would expect, the optimal value of k increases with decreasing temperature.

Surface tension values for a number of alkane systems were calculated through a combination of GC-TMMC and finite-size scaling. Our results indicate that interfacial tensions determined by using this method are consistent with estimates obtained through traditional slab-based approaches. Moreover, the com-bined TMMC-FSS technique appears to produce surface tensions with much smaller uncertainties than traditional methods. A study aimed at determining the influence of the potential cutoff distance on the surface tension indicated that interfacial tension estimates initially decrease with an increase in the cutoff

distance, with values converging to a consistent value at large enough cutoff distances. Although convergence is eventually obtained, the cutoff distances required are considerably larger than those typically employed in "standard" simulations. Certainly, a future investigation targeted toward identifying more efficient methods for calculating long-range interactions within the TMMC-FSS framework would be beneficial. Finally, surface tensions for *n*-butane, *n*-hexane, and *n*-octane were calculated with the exponential-6 model and compared with experimental data. Our results indicate that model predications overestimate the surface tension. Similar calculations with the TraPPE force field suggest that this model also overestimates the surface tension, but does so to a lesser extent than the exponential-6 model.

References and Notes

(1) Panagiotopoulos, A. Z. *Mol. Phys.* **1987**, *61*, 813.
(2) Siepmann, J. I. *Mol. Phys.* **1990**, *70*, 1145.
(3) Siepmann, J. I.; Frenkel, D. *Mol. Phys.* **1992**, *75*, 59.
(4) Frenkel, D.; Mooij, G. C. A.; Smit, B. *J. Phys.: Condens. Matter* **1992**, *4*, 3053.
(5) de Pablo, J. J.; Laso, M.; Suter, U. W. *J. Chem. Phys.* **1992**, *96*, 2395.
(6) Laso, M.; de Pablo, J. J.; Suter, U. W. *J. Chem. Phys.* **1992**, *97*, 2817.
(7) Siepmann, J. I.; Karaborni, S.; Smit, B. *Nature* **1993**, *365*, 330.
(8) Mooij, G. C. A. M.; Frenkel, D.; Smit, B. *J. Phys.: Condens. Matter* **1992**, *4*, L255.
(9) Escobedo, F.; de Pablo, J. *J. Chem. Phys.* **1996**, *105*, 4391.
(10) Jorgensen, W. L.; Madura, J. D.; Swenson, C. J. *J. Am. Chem. Soc.* **1984**, *106*, 6638.
(11) de Pablo, J. J.; Laso, M.; Siepmann, J. I.; Suter, U. W. *Mol. Phys.* **1993**, *80*, 55.
(12) Smit, B.; Karaborni, S.; Siepmann, J. I. *J. Chem. Phys.* **1995**, *102*, 2126.
(13) Martin, M. G.; Siepmann, J. I. *J. Phys. Chem. B* **1998**, *102*, 2569.
(14) Nath, S. K.; Escobedo, F. A.; de Pablo, J. J. *J. Chem. Phys.* **1998**, *108*, 9905.
(15) Errington, J. R.; Panagiotopoulos, A. Z. *J. Phys. Chem. B* **1999**, *103*, 6314.
(16) Alejandre, J.; Tildesley, D. J.; Chapela, G. A. *Mol. Phys.* **1995**, *85*, 651.
(17) Nicolas, J. P.; Smit, B. *Mol. Phys.* **2002**, *100*, 2471.
(18) Allen, M. P.; Tildesley, D. J. *Computer Simulation of Liquids*; Clarendon Press: Oxford, UK, 1987.
(19) Goujon, F. M.; Boutin, A; Fuchs, A. H. *J. Chem. Phys.* **2002**, *116*, 8106.
(20) Errington, J. R. *J. Chem. Phys.* **2003**, *119*, 3405.
(21) Fitzgerald, M.; Picard, R. R.; Silver, R. N. *Europhys. Lett.* **1999**, *46*, 282.
(22) Fitzgerald, M.; Picard, R. R.; Silver, R. N. *J. Stat. Phys.* **2000**, *98*, 321.
(23) Berg, B. A.; Neuhaus, T. *Phys. Rev. Lett.* **1992**, *61*, 9.
(24) Ferrenberg, A. M.; Swendsen, R. H. *Phys. Rev. Lett.* **1988**, *61*, 2635.
(25) Binder, K. *Phys. Rev. A* **1982**, *25*, 1699.
(26) Potoff, J. J.; Panagiotopoulos, A. Z. *J. Chem. Phys.* **2000**, *112*, 6411.
(27) Singh, J. K.; Kofke, D. A.; Errington, J. R. *J. Chem. Phys.* **2003**, *119*, 3405.
(28) Singh, J. K.; Kofke, D. A. *Mol. Simul.* **2004**, *30*, 343
(29) Singh, J. K.; Kofke, D. A. *J. Chem. Phys.* **2004**, *121*, 9574.
(30) Frenkel, D.; Smit, B. *Understanding Molecular Simulation*: *From Algorithms to Applications*, 2nd ed.; Academic Press: New York, 2002.
(31) Van der Ploeg, P.; Berendsen, H. J. C. *J. Chem. Phys.* **1982**, *76*, 3271.
(32) Errington, J. R. *Langmuir* **2004**, *20*, 3798.
(33) Errington, J. R. *Phys. Rev. E* **2003**, *67*, 012102.
(34) NIST Chemistry WebBook. http://webbook.nist.gov/chemisty.